Half-auxeticity and anisotropic transport in Pd decorated two-dimensional boron sheets

Fengxian Ma[1,#], Yalong Jiao[2,#,*], Weikang Wu[3], Ying Liu[1], Shengyuan A. Yang[3,*], Thomas Heine[2,4,5*]

[1]College of Physics, Hebei Key Laborotory of Photophysics Research and Application, Hebei Normal University, 050024 Shijiazhuang, China

[2]Faculty for Chemistry and Food Chemistry, TU Dresden, Bergstraße 66c, 01069 Dresden, Germany

[3]Research Laboratory for Quantum Materials, Singapore University of Technology and Design, 487372 Singapore, Singapore

[4]Helmholtz-Center Dresden Rossendorf, Institute of Resource Ecology, Leipzig Research Branch, 04316 Leipzig, Germany

[5]Department of Chemistry, Yonsei University, 03722 Seoul, Korea

ABSTRACT

If one strains a material, most materials shrink normal to the direction of applied strain. Similarly, if a material is compressed, it will expand in the direction orthogonal to the pressure. Few materials, those of negative Poisson ratio, show the opposite behavior. Here, we show an unprecedented feature, a material that expands normal to the direction of stress, regardless if it is strained or compressed. Such behavior, namely half-auxeticity, is demonstrated for a borophene sheet stabilized by decorating Pd atoms. We explore Pd-decorated borophene, identify three stable phases of which one has this peculiar property of half auxeticity. After carefully analyzing stability, mechanical and electronic properties we explore the origin of this very uncommon behavior, and identify it as a structural feature that may also be employed to design further 2D nanomaterials.

KEYWORDS

two-dimensional materials, auxetic materials, borophene, buckling structure, first-principle calculations

INTRODUCTION

Among a number of synthetic two-dimensional (2D) flatlands, 2D boron-based materials have sparked great scientific interest in recent research[1,2] due to their unique characteristics including structural polymorphism,[3] optical transparency[4] and versatile band structure features.[5,6] However, the trivalent outer shell of boron cannot completely occupy the in-plane sp^2 bonding state, making their structures fluxional[7] and the synthesis of 2D borophene extremely relies on the metal substrates to compensate the boron's electron-deficiency.[8] To achieve free-standing boron sheets, embedding metal atoms that can donate electrons to the boron frameworks has been considered as an effective strategy. Consequently, some metal-boron monolayers including MgB_2,[9] BeB_2,[10] FeB_2,[11] FeB_6,[12] MnB,[13] TiB_2[14] and TiB_4[15] have been designed and found to possess novel features including planar hypercoordination, Dirac cones and high Curie temperature.[11,13,15] With many intriguing chemical and physical properties, new 2D metal-boron compounds are expected to have important application potential for nanomechanics and nanoelectronics.

2D materials usually demonstrate excellent mechanical properties, often superior than their three-dimensional (3D) counterparts.[16] They are flexible and can sustain ultra-high critical strains. In recent years, 2D materials with negative Poisson's ratio (NPR) have drawn great attention due to their unconventional lattice response under compression or tension. [17-22] Poisson's ratio $\nu = -\varepsilon_{\text{trans}}/\varepsilon_{\text{axial}}$ is the negative ratio between the strain along the transverse direction $\varepsilon_{\text{trans}}$ in response to an applied uniaxial strain $\varepsilon_{\text{axial}}$. From the daily life experience, most materials would naturally contract in the transverse direction when stretched along the longitudinal direction, namely, they have a positive Poisson's ratio (PPR). In contrast, materials with NPR, also known as auxetic materials, would exhibit the rather counterintuitive behavior: they would expand (contract) laterally when a longitudinal tensile (compressive) strain is applied. As a result, such materials typically have enhanced toughness, indentation resistance and shear resistance.[23] With these exotic properties, auxetic materials display great potentials in aerospace, biomedicine, military defense and electronics.[24-26] However, compared with 3D bulks, 2D auxetic materials are still rare. Currently, the reported 2D materials with NPR can be classified into three groups, i.e. in-plane NPR (the NPR exists in $\pm x$ or $\pm y$ or other directions within the plane, e.g. penta-graphene),[27] out-of-plane NPR (the NPR exists in $\pm z$ direction, e.g. black phosphorus)[17] and bidirectional NPR (the NPR exists both in-plane and out-of-plane, e.g. Ag_2S, borophene).[28,29] Considering their enhanced mechanical performance and fascinating application potential, it is interesting to explore whether there would exist additional auxetic 2D materials, or if the lower dimensionality even offers additional surprises concerning auxetic behavior.

In this work, we performed a systematic structure search of palladium borides PdB_n (n=2,3,4)

sheets by using first-principles calculations combined with particle swarm optimization (PSO) algorithm[30,31] (see the details in the SI) and revealed a novel NPR material with intriguing mechanical and electronic properties. The 2D boron sheets were incorporated with Pd atoms because: It is a transition metal widely used in electronics (as electrodes)[32] and catalysis;[33] it can efficiently donate electrons to boron, and its 2D nanostructures are expected to be well stabilized in experiment;[34] and it has the lowest melting point among the platinum group metals,[35] which could facilitate the experimental synthesis. Finally, three low-energy Pd-B monolayers, one of PdB_4, and two of PdB_2 (PdB_2-I and PdB_2-II) stoichiometries, were discovered in this work. Importantly, the PdB_4 monolayer displays a so-far undiscovered auxetic phenomenon: along one crystal axis, the Poisson's ratio is negative for tensile strains, but becomes positive for compressive strains. As the NPR here occurs only for half of the strain parameter range, we term the effect as "half-auxeticity". To our knowledge, such phenomenon has not been reported before, and it renders PdB_4 as an attractive material with potential applications in nanomechanics. Although excellent electronic properties such as high carrier mobilities (~10^3 $cm^2 \cdot s^{-1} \cdot V^{-1}$ for the semiconducting PdB_2-I sheet) or Dirac loop (for the metallic PdB_2-II sheet) can be found in the PdB_2 monolayers (Fig. 1b and 1c), they are excluded in the following discussion due to their less interesting PPR nature. Nonetheless, as these phases are both thermodynamically stable with formation energies of -105 and -3 meV/atom, respectively, and are very likely to occur when decorating borophene, we discuss their stabilities, structural, electronic and optical properties in detail in the supporting information (Fig. S1-S7).

RESULTS AND DISCUSSION

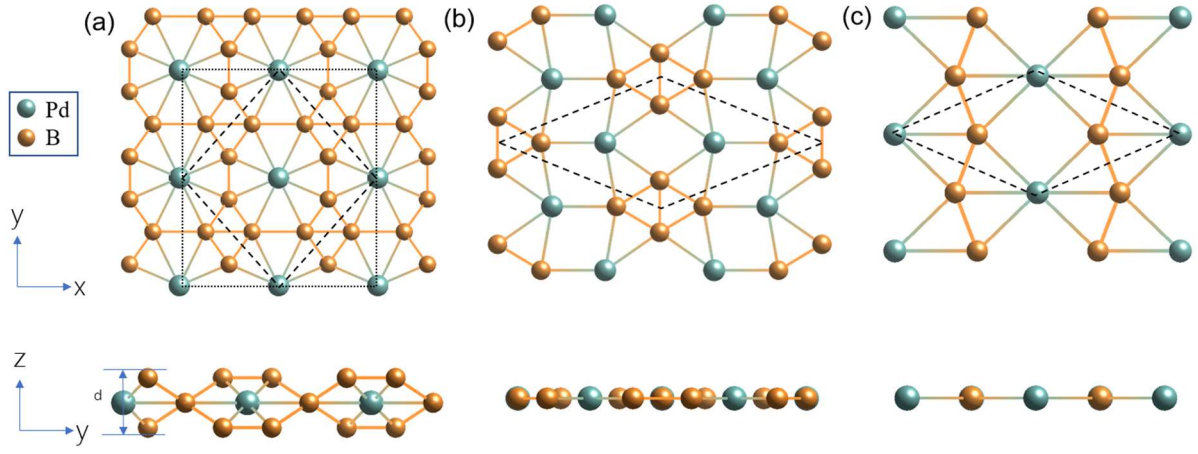

Figure 1. Top and side view of (a) PdB_4, (b) PdB_2-I (c) PdB_2-II monolayers. The dashed line represents the primitive cell for each structure. The solid line in (a) marks the double unit cell that is utilized below for the discussion of the mechanical properties.

Structure of the PdB_4 monolayer. As shown in Fig. 1a, the B atoms in PdB_4 monolayer form

a network composed of 4-membered and 8-membered rings, and more interestingly, each Pd atom is octacoordinated to B atoms, forming Pd-B_8 wheel-like structural motifs. Such peculiar hypercoordinated structures with B have been attracting great interest for a long time, originally found in molecules and clusters[36-39] and most recently extended to periodic 2D systems.[12,15] The PdB_4 phase crystallizes in the CMMA space group with in-plane anisotropy. More importantly, the structure is not completely planar, but is corrugated with a thickness (d) of 1.61 Å. As indicated in Fig. 1a, in each unit cell, four out of the eight B atoms are moved out of the 2D plane formed by other atoms, two shifted above and two shifted down. The corrugation significantly stabilizes the 2D sheet by 73.5 meV/atom, indicating the robustness of the buckled geometry. From the Bader charge analysis we find a sizable charge transfer from the Pd (0.22 e per atom) to boron atoms. According to the analysis by Pu et al.,[39] in a planar configuration, B_8 ring can only enclose smaller 3d elements, such as Mn, Fe, and Co. Pd is a 4d element with larger radius than 3d. Therefore, the observed buckling is consistent with the previous analysis, and is an intrinsic feature for the hypercoordinated Pd-B_8 wheel structure. As we shall see, the peculiar structure involving Pd hypercoordination and the B buckling plays a crucial role in generating the half-auxetic effect in PdB_4.

Stability of the PdB_4 monolayer. To access the experimental feasibility to grow the predicted PdB_4 layer, we first evaluated the thermodynamic stability by calculating the formation energy. We define the formation energy per atom E_f with respect to borophene and solid palladium: $E_f = [E(PdB_n) – xE(Pd) – yE(B)]/(x+y)$, where $E(PdB_4)$, E(Pd), and E(B) are the energy of the monolayer, the energy per atom of the solid Pd, and the energy of borophene monolayer,[1] respectively, thus to experimentally available phases of the constituting elements. The estimated E_f for PdB_4 is -42.0 meV/atom, indicating that it is a thermodynamically stable Pd-B phase, even more stable than aggregated Pd clusters at the borophene surface. Based on the elastic stability criteria[40], stable 2D lattices should satisfy: C_{11} , C_{22} , C_{66}> 0 & $C_{11} + C_{22} - 2C_{12} > 0$, where C_{ij} are the elastic constants. This criterion is met here, see Table S1 for summarized values.

There are no imaginary frequencies in the phonon dispersion (Fig. 2a), which otherwise shows the typical behavior of a kinetically stable 2D material, with two linear and one parabolic acoustic branches. The highest frequencies of PdB_4 reach up to 36.4 THz (1214 cm^{-1}), which is higher than the highest frequencies found in silicene (580 cm^{-1}),[41] Cu_2Si (420 cm^{-1}),[42] MoS_2 monolayers (473 cm^{-1}).[43] Such high-energy phonons characterize the robust Pd−B and B−B interactions in PdB_4. We further perform ab initio molecular dynamics (AIMD) simulation at 300 K, 800 K and 1200 K to evaluate the thermal stability of the PdB_4 sheet, in which a supercell containing 80 atoms was used. The snapshot taken at the end of a 10 ps simulation is presented in Fig. S2. We find the framework is well preserved at each temperature as in the original configuration, indicating it is thermally stable.

Electronic properties of the PdB_4 monolayer. PdB_4 monolayer is a semiconductor with an indirect band gap of, at the HSE06 hybrid functional level, 1.22 eV. As shown in Fig. 2b, the valence band maximum (VBM) for PdB_4 phase is along the M-Γ path, while the conduction band minimum (CBM) locates at M point. From the projected density of states (PDOS), it can be found both VBM and CBM of PdB_4 are contributed by the hybridized Pd-*d* and B-*p* states. The partial charge density distributions plotted in Fig. S5a-S5b is consistent with the PDOS results. The orbitally resolved band structures are presented in Fig. S8. The carrier mobilities of 2D materials determine their performance as electronic device components, and can be evaluated using deformation potential (DP) theory. [44] The details for the carrier mobility (μ) results for PdB_4 are provided in the SI (Fig. S9 and Table S2). For PdB_4 monolayer, the calculated electron (hole) mobility shows a significant anisotropy, along y direction is 2270 (1640) $cm^2 \cdot s^{-1} \cdot V^{-1}$, which is much larger than that along x direction (960 (43) $cm^2 \cdot s^{-1} \cdot V^{-1}$). Notably, the carrier mobilities for PdB_4 are comparable to that in phosphorene ($\sim 10^4$ $cm^2 \cdot s^{-1} \cdot V^{-1}$)[45], and higher than that of 2D transition metal dichalcogenides such as MoS_2 ($\sim 10^2$ $cm^2 \cdot s^{-1} \cdot V^{-1}$)[46], demonstrating its excellent conductivity.

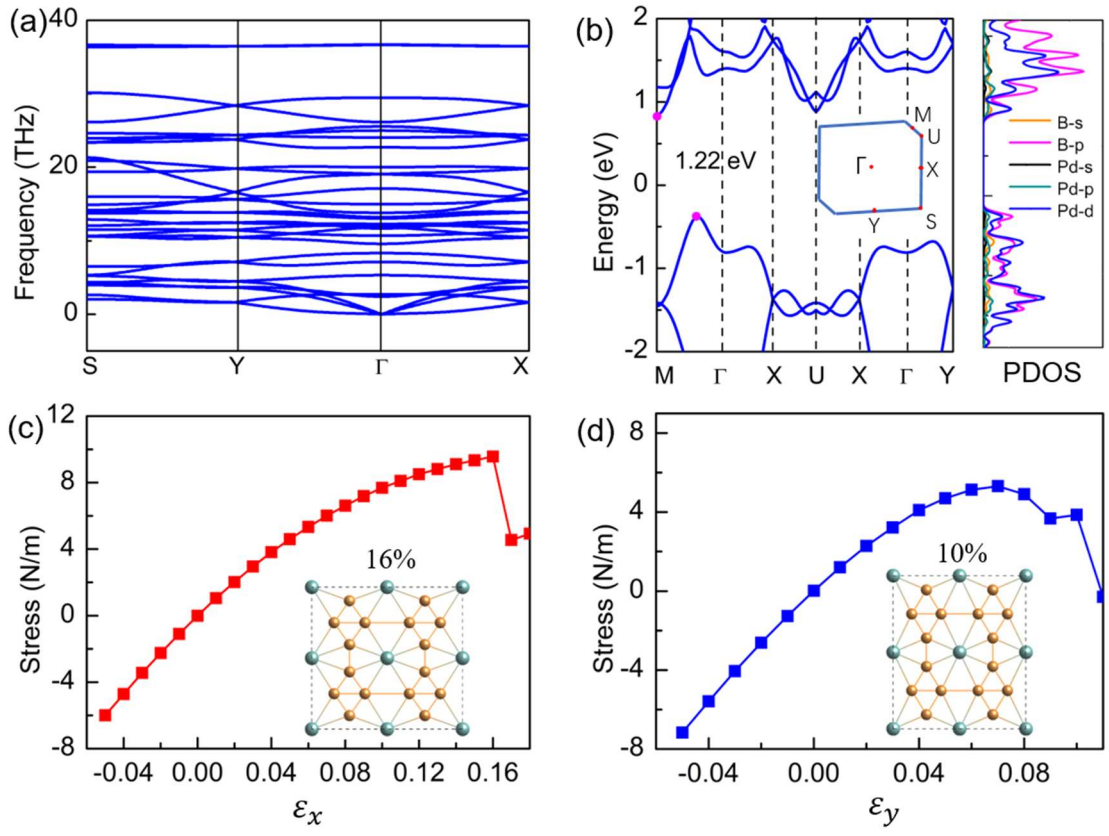

Figure 2. (a) Phonon dispersion curves for PdB_4 monolayer. (b) Band structure and PDOS for PdB_4 monolayer. Inset: The Brillouin zone (c-d) The stress-strain curves along x and y directions, respectively. Insets: The structural snapshots just before rupture under 16% and 10 % strain, respectively.

Strain effect of the PdB_4 monolayer. To understand the strain behavior of PdB_4 monolayer, we first estimated its elastic limit via stress-strain curves along x and y directions. Uniaxial strain is defined as $\varepsilon_i = \frac{l_i - l_{i0}}{l_{i0}} = \frac{\Delta l_i}{l_{i0}}$, where *i* represents a direction in the lattice (here x and y), l_{i0} denotes the equilibrium lattice constant along direction i, and l_i is its strained value. As shown in Fig. 2c, the stress rises monotonously, but slows down as the strain increases. The anisotropic mechanical responses in different directions are evident, the defect-free system can sustain an ultimate tensile strength (UTS) of 9.6 N/m along x direction with a corresponding fracture point at 16%. In comparison, the UTS and fracture point along y direction are smaller, with the value of 5.3 N/m and 10%, respectively. The estimated ultimate tensile strength is comparable to that of silicene (7.2 N/m) and germanene (4.7 N/m)[47], whereas the fracture point of the PdB_4 sheet is somewhat smaller than the referred materials (17.5% - 20.5%). Strain has a significant effect on the PdB_4 electronic properties, suggesting the material's suitability in electromechanical applications and strain sensors (see the details in the supporting information).

Mechanical properties of the PdB_4 monolayer. The unique geometries in the Pd-B_8 wheels in PdB_4 sheet show fascinating mechanical performance, and it is thus intriguing to explore them in more detail. In the elastic theory, 2D Young's moduli along x and y directions are defined by the elastic constants as $Y_x^{2D} = C_{11}C_{22} - C_{12}C_{21}/C_{22}$ and $Y_y^{2D} = C_{11}C_{22} - C_{12}C_{21}/C_{11}$, respectively. The evaluated $Y_x^{2D}$and Y_y^{2D} values are 105.7 and 121.4 GPa·nm for PdB_4, indicating mechanical anisotropy. These values are about 32% - 47% of that in 2D MoS_2 (330 GPa·nm)[48], but larger than that of phosphorene (23.0 GPa·nm along armchair and 92.3 GPa·nm along zigzag direction),[49] demonstrating that they are flexible materials. The corresponding Poisson's ratios ν at equilibrium are defined as $\nu_x^{2D} = C_{12}/C_{22};\ \nu_y^{2D} = C_{12}/C_{11}$, they are found to be negative for PdB_4 due to the negative C_{12}, indicating it is an auxetic material. Next, we explore the mechanical properties of PdB_4 monolayer under uniaxial strain. Generally, the strain disturbs the equilibrium state of the structure, thus the total energy of the system will rise (see strain-energy curve in Fig. S12). To provide an overall picture, the resultant strains (including both in-plane and vertical directions) in response to uniaxial deformation ranging from −8% to 8% are plotted by using a rectangular unit cell. The same data is utilized to calculate the Poisson's ratio is calculated by the ration of the strain derivatives $\nu = -\frac{d\varepsilon_1}{d\varepsilon_2}$. From Figs. 3b and 3d one can see that the layer thickness (strain along *z*) decreases with the increase of the in-plane strain (along *x* and *y*), indicating the out-of-plane Poisson's ratios in PdB_4 sheet are always positive. To explore the in-plane Poisson's ratios, we consider uniaxial deformation of the sheet along *x* and monitor the change along *y*. Figure 3a shows that the Poisson ratio remains close to zero, with slightly negative values (NPR). Thus, for

expansion in *x* direction, no appreciable strain is expected for y direction.

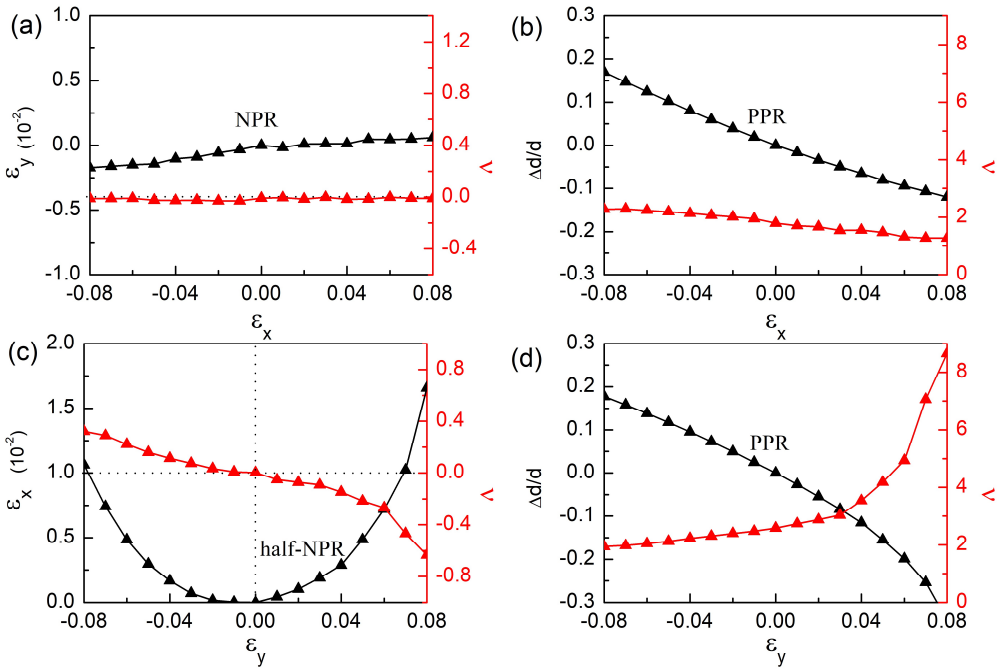

Figure 3. Mechanical response and calculated Poisson's ratio ν of PdB_4 monolayer under uniaxial strain along (a-b) x- and (c-d) y-directions. In the calculation, a rectangular cell was used.

Remarkably, the in-plane Poisson's ratio in the *y* direction shows a distinct behavior. Under tensile strain along *y* direction, the lateral dimension along *x* will expand, as shown in Fig. 3c. This gives a negative Poisson's ratio. Normally, an auxetic material would contract under a compressive strain, i.e., the Poisson's ratio maintains the same sign for negative strain (although its absolute value may change). Surprisingly, for PdB_4, under a compressive *y*-strain, the lattice size along *x* displays a response opposite to our expectation, i.e. it increases with a positive Poisson's ratio. Note that the evolution of Poisson's ratio is linear within about 4% strain, with negative slope, and crosses the zero line at the equilibrium position. We call this behavior the half-auxetic effect. With this effect, PdB_4 exhibits the peculiar behavior that it always expands along *x* whenever it is strained along *y*, regardless of whether this strain is tensile or compressive.

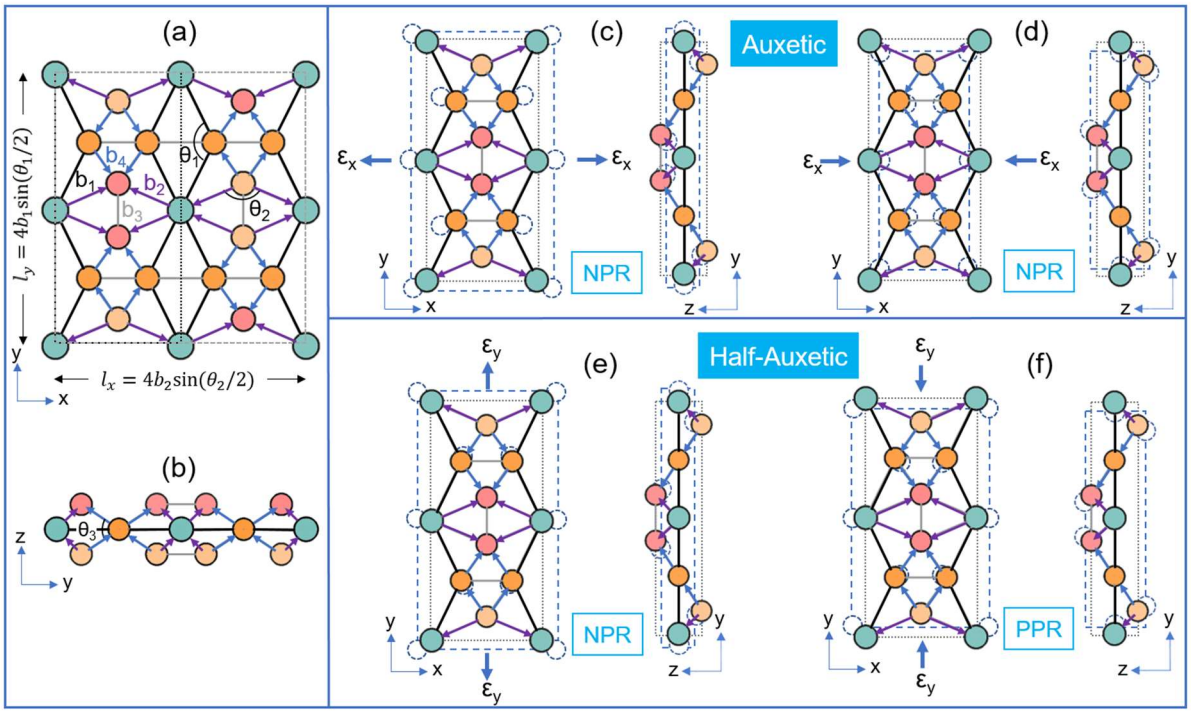

Figure 4. (a-b) Top and side view of the unit cell of the strain-free PdB_4 monolayer. All Pd atoms are within the z=0 plane. Boron atoms above, in, and below z=0 plane are represented by light red, orange and light orange colors, respectively. Four distinct bond types are indicated, i.e. in-plane Pd-B bonds b_1 (black lines) and B-B bonds b_3 (grey lines), out-of-plane Pd-B bonds b_2 (purple arrows) and B-B bonds b_4 (blue arrows). Arrows always point out upwards along z direction. Two types of Pd-B-Pd angles are labelled as θ_1 and θ_2, respectively. θ_3 shown in (b) is the projection of a dihedral angle. For simplicity, only half of the cell is adopted for the following discussion, the other half-cell can be obtained by straight-forward symmetry operations. (c-f) The atomic displacements (enlarged for better visibility) for PdB_4 monolayer during compressive and tensile strain along x and y directions. Dotted/dashed lines represent the lattice before/after strain. Dashed circles indicate the positions of atoms under strain.

Origin of the (half-) auxetic properties of PdB_4 monolayer.

Figure 4 relates the lattice vectors in x and y directions to chemically relevant bonding data. While both lattice vectors in the rectangular cell directly relate to Pd-Pd distances, the connectivity in the bonded network is slightly more involved. Along x direction, the tensile force puts significant stress on b_2 (Fig. 4c). To avoid energy-costly bond length stretching, the corrugation of the sheet reduces, expressed by θ_3, the projection of a dihedral angle (see Figure 4b). This pushes the neighboring in-plane atoms away, triggers a stretch in both x- and y directions, and consequently increases l_y, which causes the NPR. With the same argumentation (Fig. 4d), compressing along x is best accommodated by increasing the corrugation, that is, by increasing θ_3. This pushes the b_2 bond out-of-plane and reduces l_y.

When the tension along y direction is applied (Fig. 4e), it puts stress mainly on b_1, but also on b_3. A PPR system would just react by increasing angle θ_1, in PdB_4, however, the stress is accommodated by reducing θ_3, which lowers the out-of-plane atoms and the atoms are pushed along b_2 and b_3 to slightly expand in x direction. As for the compressive strain along y direction (Fig. 4f), beyond the equilibrium position, the angles θ_2, and θ_3 are already quite large, so stronger corrugation does not yield compression along y. Instead, the system reacts in lowering θ_1, which results in a system with the typical PPR.

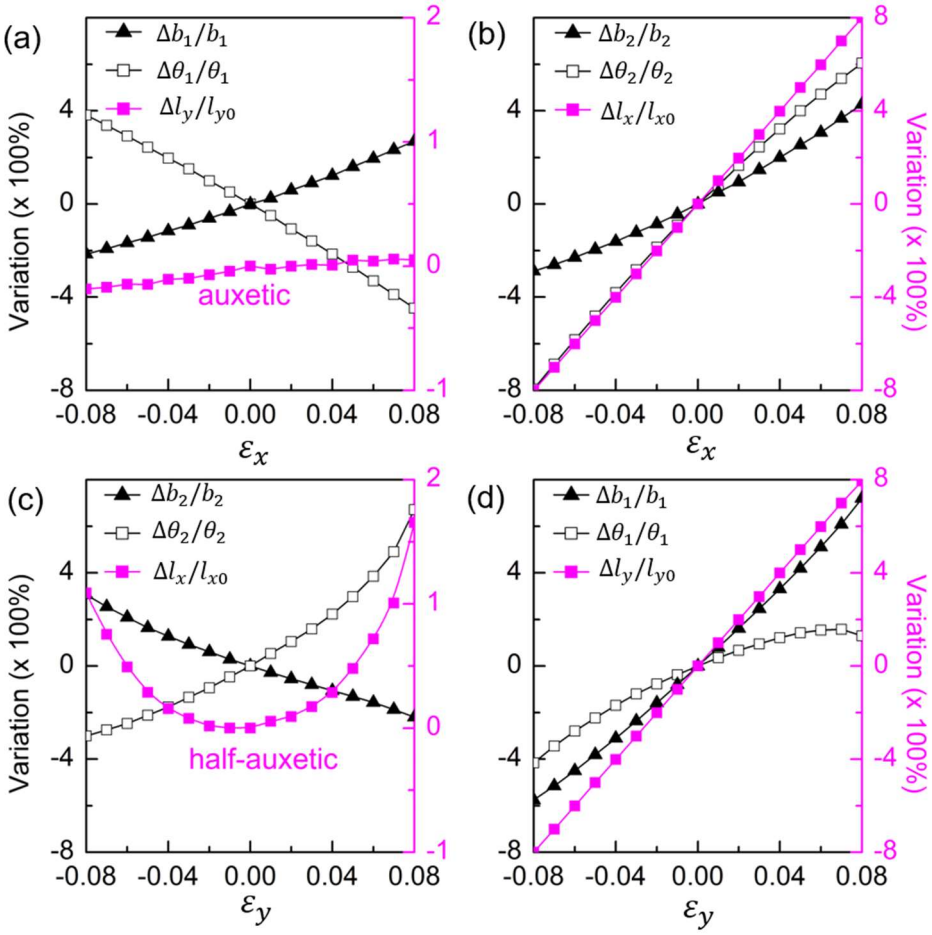

Figure 5. Dependence of the strain along x and y directions (ε_x and ε_y) of the bonding parameters b_1, b_2, θ_1 and θ_2 (for definitions, see Figure 4a). The lattice vector length l_x and l_y were obtained directly through equations $l_x = 4b_2 \sin\frac{\theta_2}{2}$ and $l_y = 4b_1 \sin\frac{\theta_1}{2}$, respectively.

To understand the auxetic behavior at the atomistic level, the interdependence of deformation and geometric parameters is shown in Fig. 5. We map the lattice constants to geometric parameters that are directly related to the structural change resulting from strain: $l_x =$

$4b_2 \sin\frac{\theta_2}{2}$, $l_y = 4b_1 \sin\frac{\theta_1}{2}$, i.e. to the Pd-B bond lengths b_1 and b_2 and the Pd-B-Pd angles θ_1 and θ_2. Clearly, the NPR along x direction is main attributed by b_1 and θ_1 (Fig. 5a). Particular interest can be seen in Fig. 5c. Specifically, during tension, the slope of θ_2 is much larger than that of b_2. The variation of θ_2 is therefore the dominant factor, and l_x follows its increasing trend. During compression, however, the change of θ_2 becomes much slower and the increased b_2 overwhelms the decreased θ_2, leading to the unconventional increased l_x (pink curve). In short, the half-auxecticity in PdB_4 layer is mainly due to the competition between the geometric parameters (b_2 and θ_2). Furthermore, movies for PdB_4 monolayer under tensile/compressive strain y have been made. To visualize the half-auxeticity more clearly, the displacements of atoms along x direction were manually enlarged ten times (see supporting movie files).

CONCLUSION

We presented an unprecedented phenomenon in 2D materials, a material that changes sign in its Poisson ratio precisely at the equilibrium position. By screening 2D palladium borides, where Pd adatoms increase layer stability by balancing the electron deficiency of borophene, three phases of particularly high chemical, dynamical and mechanical stabilities have been identified. Among them, PdB_4 shows besides high electronic mobilities and lattice anisotropy and unprecedented feature, namely half-auxetic behaviour: while it has a very small negative Poisson's ratio for strain along the x axis (as defined in Figure 4), for deformation along y axis Poisson's ratio changes sign at the equilibrium distance, and the material expands along x irrespective if it is compressed or expanded along y. Thus, it changes its character from an auxetic material (negative Poisson's ratio) for tensile stress along y, towards the common non-auxetic character (positive Poisson's ratio) when compressed along y. This unprecedented mechanical property is mapped to distinct features of the bonding pattern of PdB_4 and we can expect that other materials with a similar behavior can be designed.

As electronic and mechanical properties are strongly coupled, electromechanical PdB_4 devices may serve as ideal pilots to explore the characteristics of half-auxetic materials.

ASSOCIATED CONTENT

Supporting Information

The Supporting Information is available free of charge.

Supplementary results including computational details of this work, AIMD simulations, elastic constants and structural information for all predicted structures, the phonon spectrum, band structures, PDOS, partial charge density distributions and light absorbance for the PdB_2 monolayers, movies, orbitally resolved band structure, electronic properties and elastic energy of PdB_4 monolayer under strain effect.

AUTHOR INFORMATION

Corresponding Authors

*E-mail: yalong.jiao@mailbox.tu-dresden.de (Y.J.)
*E-mail: shengyuan_yang@sutd.edu.sg (S.A.Y.)
*E-mail: thomas.heine@tu-dresden.de (T.H.)

Notes

[#] These authors contributed equally. The authors declare no competing financial interest.

ACKNOWLEDGMENT

F.M. acknowledges the support from the National Natural Science Foundation of China (Grant No. 11847017 and 11904077), Science Foundation of Hebei Normal University (Grant No. L2019B09) and financial support program from Hebei Province (Grant No. E2019050018). Y. J. appreciates the funding from the Alexander von Humboldt-Foundation. S. A. Y. is supported by the Singapore MOE AcRF Tier 2 (Grant No. MOE2019-T2-1-001). The high-performance computer center of TU Dresden (ZIH) is thanked for computer time.

REFERENCES

(1) Mannix, A. J.; Zhou, X.-F.; Kiraly, B.; Wood, J. D.; Alducin, D.; Myers, B. D.; Liu, X.; Fisher, B. L.; Santiago, U.; Guest, J. R.; Yacaman, M. J.; Ponce, A.; Oganov, A. R.; Hersam, M. C.; Guisinger, N. P. Synthesis of borophenes: Anisotropic, two-dimensional boron polymorphs. *Science* **2015**, *350*, 1513-1516.

(2) Feng, B.; Zhang, J.; Zhong, Q.; Li, W.; Li, S.; Li, H.; Cheng, P.; Meng, S.; Chen, L.; Wu, K. Experimental realization of two-dimensional boron sheets. *Nature Chemistry* **2016**, *8*, 563-568.

(3) Wu, X.; Dai, J.; Zhao, Y.; Zhuo, Z.; Yang, J.; Zeng, X. C. Two-dimensional boron monolayer sheets. *ACS nano* **2012**, *6*, 7443-7453.

(4) Adamska, L.; Sadasivam, S.; Foley IV, J. J.; Darancet, P.; Sharifzadeh, S. First-principles investigation of borophene as a monolayer transparent conductor. *The Journal of Physical Chemistry C* **2018**, *122*, 4037-4045.

(5) Feng, B.; Sugino, O.; Liu, R.-Y.; Zhang, J.; Yukawa, R.; Kawamura, M.; Iimori, T.; Kim, H.; Hasegawa, Y.; Li, H.; Chen, L.; Wu, K.; Kumigashira, H.; Komori, F.; Chiang, T.-C.; Meng, S.; Matsuda, I. Dirac Fermions in Borophene. *Physical Review Letters* **2017**, *118*, 096401.

(6) Ma, F.; Jiao, Y.; Gao, G.; Gu, Y.; Bilic, A.; Chen, Z.; Du, A. Graphene-like Two-Dimensional Ionic Boron with Double Dirac Cones at Ambient Condition. *Nano Letters* **2016**, *16*, 3022-3028.

(7) Jalife, S.; Liu, L.; Pan, S.; Cabellos, J. L.; Osorio, E.; Lu, C.; Heine, T.; Donald, K. J.; Merino, G.

Dynamical behavior of boron clusters. *Nanoscale* **2016**, *8*, 17639-17644.

(8) Liu, Y.; Penev, E. S.; Yakobson, B. I. Probing the Synthesis of Two-Dimensional Boron by First-Principles Computations. **2013**, *52*, 3156-3159.

(9) Tang, H.; Ismail-Beigi, S. First-principles study of boron sheets and nanotubes. *Physical Review B* **2010**, *82*, 115412.

(10) Zhang, P.; Crespi, V. H. Theory of ${\mathrm{B}}_{\mathrm{2}}\mathrm{O}$ and ${\mathrm{B}\mathrm{e}\mathrm{B}}_{2}$ Nanotubes: New Semiconductors and Metals in One Dimension. *Physical Review Letters* **2002**, *89*, 056403.

(11) Zhang, H.; Li, Y.; Hou, J.; Du, A.; Chen, Z. Dirac State in the FeB2 Monolayer with Graphene-Like Boron Sheet. *Nano Letters* **2016**, *16*, 6124-6129.

(12) Zhang, H.; Li, Y.; Hou, J.; Tu, K.; Chen, Z. FeB_6 Monolayers: The Graphene-like Material with Hypercoordinate Transition Metal. *Journal of the American Chemical Society* **2016**, *138*, 5644-5651.

(13) Jiang, Z.; Wang, P.; Jiang, X.; Zhao, J. MBene (MnB): a new type of 2D metallic ferromagnet with high Curie temperature. *Nanoscale Horizons* **2018**, *3*, 335-341.

(14) Zhang, L. Z.; Wang, Z. F.; Du, S. X.; Gao, H. J.; Liu, F. Prediction of a Dirac state in monolayer ${\mathrm{TiB}}_{2}$. *Physical Review B* **2014**, *90*, 161402.

(15) Qu, X.; Yang, J.; Wang, Y.; Lv, J.; Chen, Z.; Ma, Y. A two-dimensional TiB4 monolayer exhibits planar octacoordinate Ti. *Nanoscale* **2017**, *9*, 17983-17990.

(16) Akinwande, D.; Brennan, C. J.; Bunch, J. S.; Egberts, P.; Felts, J. R.; Gao, H.; Huang, R.; Kim, J.-S.; Li, T.; Li, Y. J. E. M. L. A review on mechanics and mechanical properties of 2D materials—Graphene and beyond. *Extreme Mechanics Letters* **2017**, *13*, 42-77.

(17) Jiang, J.-W.; Park, H. S. Negative poisson's ratio in single-layer black phosphorus. *Nature Communications* **2014**, *5*, 4727.

(18) Zhang, S.; Zhou, J.; Wang, Q.; Chen, X.; Kawazoe, Y.; Jena, P. Penta-graphene: A new carbon allotrope. *Proceedings of the National Academy of Sciences* **2015**, *112*, 2372-2377.

(19) Wang, Y.; Li, F.; Li, Y.; Chen, Z. Semi-metallic Be_5C_2 monolayer global minimum with quasi-planar pentacoordinate carbons and negative Poisson's ratio. *Nature Communications* **2016**, *7*, 11488.

(20) Peng, R.; Ma, Y.; Wu, Q.; Huang, B.; Dai, Y. Two-dimensional materials with intrinsic auxeticity: progress and perspectives. *Nanoscale* **2019**, *11*, 11413-11428.

(21) Jiang, J.-W.; Chang, T.; Guo, X.; Park, H. S. Intrinsic Negative Poisson's Ratio for Single-Layer Graphene. *Nano Letters* **2016**, *16*, 5286-5290.

(22) Gao, Z.; Dong, X.; Li, N.; Ren, J. Novel Two-Dimensional Silicon Dioxide with in-Plane Negative Poisson's Ratio. *Nano Letters* **2017**, *17*, 772-777.

(23) Fang, R.; Cui, X.; Stampfl, C.; Ringer, S. P.; Zheng, R. Negative Poisson's ratio in 2D life-boat structured crystals. *Nanoscale Advances* **2019**, *1*, 1117-1123.

(24) Scarpa, F.; Yates, J.; Ciffo, L.; Patsias, S. J. P. o. t. I. o. M. E., Part C: Journal of Mechanical Engineering Science. Dynamic crushing of auxetic open-cell polyurethane foam. **2002**, *216*, 1153-1156.

(25) Friis, E. A.; Lakes, R. S.; Park, J. B. Negative Poisson's ratio polymeric and metallic foams. *Journal of Materials Science* **1988**, *23*, 4406-4414.

(26) Alderson, A.; Alderson, K. J. P. o. t. I. o. M. E., Part G: Journal of Aerospace Engineering. Auxetic materials. **2007**, *221*, 565-575.

(27) Zhang, S.; Zhou, J.; Wang, Q.; Chen, X.; Kawazoe, Y.; Jena, P. Penta-graphene: A new carbon allotrope. **2015**, *112*, 2372-2377.

(28) Peng, R.; Ma, Y.; He, Z.; Huang, B.; Kou, L.; Dai, Y. Single-Layer Ag2S: A Two-Dimensional

Bidirectional Auxetic Semiconductor. *Nano Letters* **2019**, *19*, 1227-1233.

(29) Kou, L.; Ma, Y.; Tang, C.; Sun, Z.; Du, A.; Chen, C. Auxetic and Ferroelastic Borophane: A Novel 2D Material with Negative Possion's Ratio and Switchable Dirac Transport Channels. *Nano Letters* **2016**, *16*, 7910-7914.

(30) Wang, Y.; Lv, J.; Zhu, L.; Ma, Y. Crystal structure prediction via particle-swarm optimization. *Phys. Rev. B* **2010**, *82*, 094116.

(31) Wang, Y.; Lv, J.; Zhu, L.; Ma, Y. CALYPSO: A method for crystal structure prediction. *Comput. Phys. Commun.* **2012**, *183*, 2063-2070.

(32) Wang, J.-Y.; Zhang, H.-X.; Jiang, K.; Cai, W.-B. From HCOOH to CO at Pd Electrodes: A Surface-Enhanced Infrared Spectroscopy Study. *Journal of the American Chemical Society* **2011**, *133*, 14876-14879.

(33) Nishihata, Y.; Mizuki, J.; Akao, T.; Tanaka, H.; Uenishi, M.; Kimura, M.; Okamoto, T.; Hamada, N. Self-regeneration of a Pd-perovskite catalyst for automotive emissions control. *Nature* **2002**, *418*, 164-167.

(34) Noh, J.-S.; Lee, J. M.; Lee, W. Low-dimensional palladium nanostructures for fast and reliable hydrogen gas detection. *Sensors* **2011**, *11*, 825-851.

(35) Rao, C. R. K.; Trivedi, D. C. Chemical and electrochemical depositions of platinum group metals and their applications. *Coordination Chemistry Reviews* **2005**, *249*, 613-631.

(36) Romanescu, C.; Galeev, T. R.; Li, W.-L.; Boldyrev, A. I.; Wang, L.-S. Transition-Metal-Centered Monocyclic Boron Wheel Clusters (M©Bn): A New Class of Aromatic Borometallic Compounds. *Accounts of Chemical Research* **2013**, *46*, 350-358.

(37) Islas, R.; Heine, T.; Ito, K.; Schleyer, P. v. R.; Merino, G. Boron Rings Enclosing Planar Hypercoordinate Group 14 Elements. *Journal of the American Chemical Society* **2007**, *129*, 14767-14774.

(38) Ito, K.; Pu, Z.; Li, Q.-S.; Schleyer, P. v. R. Cyclic Boron Clusters Enclosing Planar Hypercoordinate Cobalt, Iron, and Nickel. *Inorganic Chemistry* **2008**, *47*, 10906-10910.

(39) Pu, Z.; Ito, K.; Schleyer, P. v. R.; Li, Q.-S. Planar Hepta-, Octa-, Nona-, and Decacoordinate First Row d-Block Metals Enclosed by Boron Rings. *Inorganic Chemistry* **2009**, *48*, 10679-10686.

(40) Wu, Z.-j.; Zhao, E.-j.; Xiang, H.-p.; Hao, X.-f.; Liu, X.-j.; Meng, J. Crystal structures and elastic properties of superhard IrN_2 and IrN_3 from first principles. *Physical Review B* **2007**, *76*, 054115.

(41) Cahangirov, S.; Topsakal, M.; Aktürk, E.; Şahin, H.; Ciraci, S. Two-and one-dimensional honeycomb structures of silicon and germanium. *Physical Review Letters* **2009**, *102*, 236804.

(42) Yang, L.-M.; Bačić, V.; Popov, I. A.; Boldyrev, A. I.; Heine, T.; Frauenheim, T.; Ganz, E. Two-Dimensional Cu_2Si Monolayer with Planar Hexacoordinate Copper and Silicon Bonding. *Journal of the American Chemical Society* **2015**, *137*, 2757-2762.

(43) Molina-Sanchez, A.; Wirtz, L. Phonons in single-layer and few-layer MoS_2 and WS_2. *Physical Review B* **2011**, *84*, 155413.

(44) Bardeen, J.; Shockley, W. Deformation Potentials and Mobilities in Non-Polar Crystals. *Physical Review* **1950**, *80*, 72-80.

(45) Qiao, J.; Kong, X.; Hu, Z.-X.; Yang, F.; Ji, W. High-mobility transport anisotropy and linear dichroism in few-layer black phosphorus. *Nature Communications* **2014**, *5*, 4475.

(46) Rawat, A.; Jena, N.; Dimple; De Sarkar, A. A comprehensive study on carrier mobility and artificial photosynthetic properties in group VI B transition metal dichalcogenide monolayers. *Journal of Materials Chemistry A* **2018**, *6*, 8693-8704.

(47) Mortazavi, B.; Rahaman, O.; Makaremi, M.; Dianat, A.; Cuniberti, G.; Rabczuk, T. First-principles

investigation of mechanical properties of silicene, germanene and stanene. *Physica E: Low-dimensional Systems and Nanostructures* **2017**, *87*, 228-232.

(48) Castellanos-Gomez, A.; Poot, M.; Steele, G. A.; van der Zant, H. S. J.; Agraït, N.; Rubio-Bollinger, G. Elastic Properties of Freely Suspended MoS_2 Nanosheets. **2012**, *24*, 772-775.

(49) Wang, L.; Kutana, A.; Zou, X.; Yakobson, B. I. Electro-mechanical anisotropy of phosphorene. *Nanoscale* **2015**, *7*, 9746-9751.

Table of Contents